THE JOURNAL OF PHYSICAL CHEMISTRY A

Article

pubs.acs.org/JPCA

Luminescence and Energy Transfer in $Lu_3Al_5O_{12}$ Scintillators Co-Doped with Ce^{3+} and Tb^{3+}

Joanna M. Ogiegło,[†] Aleksander Zych,[†] Konstantin V. Ivanovskikh,[†,‡] Thomas Jüstel,[§] Cees R. Ronda,*[,†,∥,⊥] and Andries Meijerink[†]

[†]CMI, Debye Institute for Nanomaterials Science, Utrecht University, P O. Box 80 000, 3508 TA Utrecht, The Netherlands

[‡]Department of Physics and Astronomy, University of Canterbury, Private Bag 4800, Christchurch 8020, New Zealand

[§]University of Applied Sciences Münster, 48565 Steinfurt, Germany

[∥]Philips Research Europe-Eindhoven, High Tech Campus 4, 5656 AE Eindhoven, The Netherlands

[⊥]Centre for Optical and Electromagnetic Research, Zhejiang University, Hangzhou 310058, China

ABSTRACT: $Lu_3Al_5O_{12}$ (LuAG) doped with Ce^{3+} is a promising scintillator material with a high density and a fast response time. The light output under X-ray or γ-ray excitation is, however, well below the theoretical limit. In this paper the influence of codoping with Tb^{3+} is investigated with the aim to increase the light output. High resolution spectra of singly doped LuAG (with Ce^{3+} or Tb^{3+}) are reported and provide insight into the energy level structure of the two ions in LuAG. For Ce^{3+} zero-phonon lines and vibronic structure are observed for the two lowest energy 5d bands and the Stokes' shift (2 350 cm^{-1}) and Huang−Rhys coupling parameter (S = 9) have been determined. Tb^{3+} 4f−5d transitions to the high spin (HS) and low spin (LS) states are observed (including a zero-phonon line and vibrational structure for the high spin state). The HS−LS splitting of 5400 cm^{-1} is smaller than usually observed and is explained by a reduction of the 5d−4f exchange coupling parameter J by covalency. Upon replacing the smaller Lu^{3+} ion with the larger Tb^{3+} ion, the crystal field splitting for the lowest 5d states increases, causing the lowest 5d state to shift below the $^5D_4$ state of Tb^{3+} and allowing for efficient energy transfer from Tb^{3+} to Ce^{3+} down to the lowest temperatures. Luminescence decay measurements confirm efficient energy transfer from Tb^{3+} to Ce^{3+} and provide a qualitative understanding of the energy transfer process. Co-doping with Tb^{3+} does not result in the desired increase in light output, and an explanation based on electron trapping in defects is discussed.

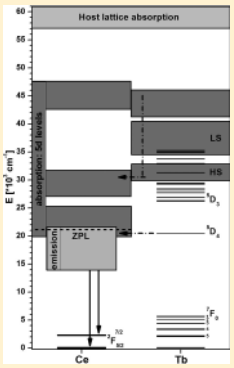

I. INTRODUCTION

The field of medical imaging develops rapidly. New imaging techniques and improvement of existing techniques benefit from materials research aimed at higher sensitivity and resolution as well as increasing the safety and comfort of patients.[1] Computed Tomography (CT) is an important tool in the diagnosis of diseases. It relies on the creation of 3D-images of the body based on cross sections created by a rapidly revolving scanning X-ray source and detector array around the patient. A crucial component in the detector array are scintillator crystals that convert high energy (X-ray) radiation into visible light that is detected by photodiodes or photomultipliers.[2]

An important class of scintillators are aluminum garnets doped with lanthanide ions. The garnets have good chemical and radiation stability, have excellent mechanical properties, and show efficient luminescence when doped with lanthanide ions. Because of their cubic structure it is possible to prepare highly transparent scintillators by pressing of polycrystalline material. Scintillators made as transparent ceramics have important benefits over single crystals (lower cost, higher flexibility, reduced fracture risk).[3] Of the various garnets, $Lu_3Al_5O_{12}$ (lutetium aluminum garnet, LuAG) has a high density (ρ_{LuAG} = 6.73 g/cm^3) and high effective atomic number (Z_{eff} = 60) and therefore high stopping power. This makes LuAG more attractive as a scintillator host lattice than the lower density $Y_3Al_5O_{12}$ (yttrium aluminum garnet, YAG), which was investigated extensively in the past 30 years for various applications.[4]

LuAG doped with Ce^{3+} (LuAG:Ce) is regarded as a particularly promising scintillator due to its allowed electric-dipole 5d−4f transition and high theoretical light yield (LY). On the basis of the Bartram−Lempicki model, the maximum LY has been calculated to be 60 000 photons/MeV.[5] However, experimental studies report lower values for the LY of LuAG:Ce and YAG:Ce which were 12 500 and 25 000 photons/MeV, respectively.[6] The discrepancy may be related to native defects in the host lattice (vacancies, antisites, dislocations), which trap electrons and holes that recombine nonradiatively.[7] In addition to a low efficiency, some afterglow is also observed, which also points to a role of defects in the garnets.[8]

To compete with trapping by defects, a higher activator concentration may be used. However, increasing the Ce^{3+}

Received: February 9, 2012
Revised: May 19, 2012
Published: July 26, 2012

ACS Publications © 2012 American Chemical Society

concentration will lead to concentration quenching: the excitation energy will be transferred between Ce^{3+} neighbors, which leads to energy migration to defects.[9] Concentration quenching is commonly observed at high activator concentrations. A possible solution to improve the energy flow from the host lattice to the emitting Ce^{3+} ions is the introduction of a coactivator ,which can capture the excitation energy (by capturing excitons) and transfers the excitation energy efficiently to Ce^{3+}. The choice of a suitable coactivator can be guided by the analysis of the Dieke diagram for trivalent rare earth ions. Figure 1 presents the Dieke diagram where the 4f−5d absorption and emission bands of Ce^{3+} in LuAG are marked.

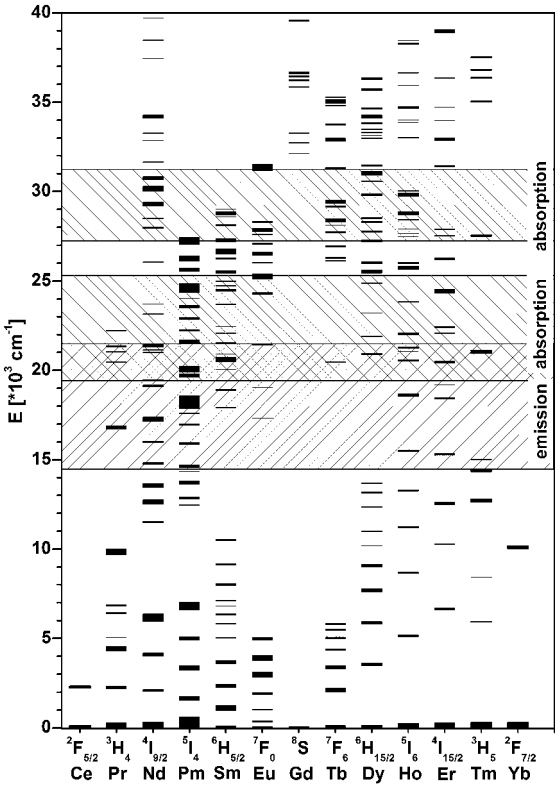

Figure 1. Dieke diagram of trivalent rare earth ions with 4f−5d absorption and 5d−4f emission bands of Ce^{3+} indicated.

A suitable coactivator should be characterized by absorption levels located between absorption of the host lattice and Ce^{3+} emission. In addition, its emission should overlap with Ce^{3+} absorption. At high coactivator concentrations an efficient capture of the host electronic excitations (electron−hole pairs or excitons)[10] created under high energy excitation will occur by the coactivator ions and will be followed by energy transfer to Ce^{3+}. Analysis of the diagram in Figure 1 shows that Pr^{3+}, Tb^{3+}, and Tm^{3+} are possible coactivators because the emitting levels $^3P_0$, $^5D_4$, and $^1G_4$ of Pr^{3+}, Tb^{3+}, and Tm^{3+}, respectively, overlap with Ce^{3+} absorption band around 450 nm. For Tm^{3+} and Tb^{3+} there is also the overlap with the second 5d band for the higher energy 4f levels which may enhance energy transfer to Ce^{3+}.

In this paper the potential of Tb^{3+} as a coactivator is explored and the energy transfer processes in LuAG:Ce,Tb are investigated. To gain insight into the energy transfer processes, also high resolution spectra were recorded at low temperatures and luminescence lifetime measurements of the Ce^{3+} and Tb^{3+} emission were performed. The results show that the $^5D_4$ level of Tb^{3+} is very close in energy to the lowest 5d level of Ce^{3+}. Efficient donor−acceptor energy transfer takes place from Tb^{3+} to Ce^{3+}, but this does not result in an enhanced light output under high energy excitation.

II. PREPARATION AND CHARACTERIZATION

A. Synthesis. All materials investigated were prepared using a modified Pechini method as described by Katelnikovas et al.[11] using high purity reagents (at least 99.999%). Lu_2O_3, $Al(NO_3)_3{\cdot}9H_2O$, $Pr(NO_3)_3{\cdot}6H_2O$, and $Ce(NO_3)_3{\cdot}6H_2O$ were used as starting materials. Citric acid was used as the polymerizing agent. The calcinations were performed in two steps at 1000 °C for 3 h and 1650 °C for 4 h with an intermediate grinding step. To obtain Ce and Tb ions in the trivalent state, the annealing was carried out under CO. Single crystalline phase formation in all samples was confirmed with the X-ray diffraction (XRD) measurements recorded on Rigaku Miniflex II diffractometer. On the basis of the XRD patterns, it was concluded that the samples are phase pure and, for the mixed (Lu,Tb) compositions, solid solutions are formed on the basis of the continuous shift of the XRD lines upon substitution of Lu by Tb.

B. Optical Spectroscopy. Luminescence spectra were recorded between 1.5 and 300 K on an Edinburgh Instruments FLS 920 spectrofluorometer using a 450 W Xe lamp as excitation source. The spectra were measured with a resolution of 0.05 to 1 nm. Low-temperature measurements were done using an Oxford Instruments liquid helium flow cryostat. Luminescence decay traces were recorded using a picosecond diode laser at 406 nm in combination with time-correlated photon counting using a TimeHarp card (for decays in the ns regime), excitation with 10 ns pulses at 355 nm from a frequency-tripled YAG-laser in combination with a Tektronix 2 440 digital oscilloscope (in the μs regime) and flashlamp excitation at 280 nm using a multichannel scaling card for decays in the ms time regime. Radioluminescence (RL) measurements were performed in reflection geometry using Ocean Optics HR2000 CG spectrometer (with a CCD detector) coupled to a 600 μm fiber optics and a 74-UV collimating lens to collect the light more efficiently. The resolution of the system was about 1.2 nm. Dedicated Ocean Optics SpectraSuite software was used to process the measurements. The counting time was 250 ms. White X-rays from a copper X-ray lamp of a DRON diffractometer were used as the excitation source. RL efficiencies of the materials studied were calculated against a commercial Gd_2O_2S:Eu (GOS) phosphor from Phosphor Technology (UKL63/F-R1, D_{av} = 4.0 μm).

III. RESULTS AND DISCUSSION

To understand the energy flow in the codoped LuAG:Ce,Tb samples, a good spectroscopic characterization of singly doped LuAG:Ce and LuAG:Tb is required. In sections III.A and III.B the optical properties of the singly doped samples are reported and discussed. In section III.C the luminescence properties, including luminescence lifetime measurements, for the codoped sample LuAG:Ce,Tb are reported as well as light yield measurements under X-ray excitation.

A. LuAG:Ce. From the Dieke diagram shown in Figure 1 it is clear that the position of the lowest energy 5d state for Ce^{3+} is very close in energy to the $^5D_4$ level of Tb^{3+}. The position of

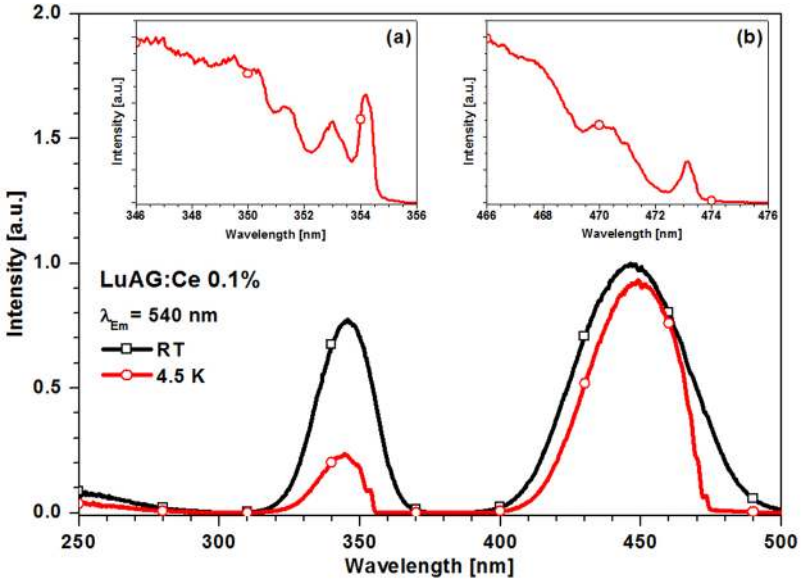

Figure 2. Excitation spectra of the Ce^{3+} emission at 540 nm in LuAG:Ce0.1% at 4.5 K and RT. Insets a and b show higher resolution 4.5 K spectra around the onset of the two lowest energy 5d excitation bands.

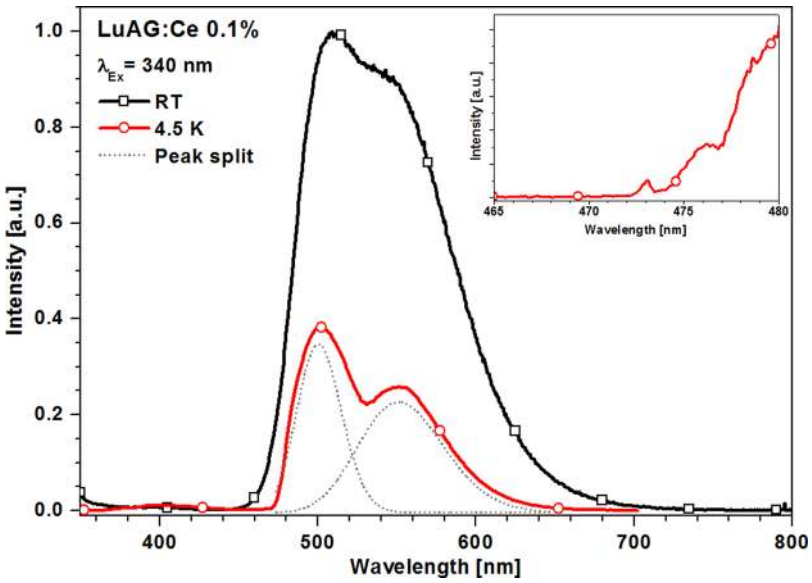

Figure 3. Emission spectrum for LuAG:Ce0.1% recorded at 4.5 K (λ_{exc} = 340 nm). The inset shows the fine structure in the onset of the emission in more detail.

the 5d state has been accurately determined for Ce^{3+} in YAG, where the zero-phonon line (ZPL) for the lowest energy 5d state is at 489.2 nm.[9,12] Because the 5d state is very sensitive to small variations in the local coordination, which affect the covalency and the crystal field (CF) splitting, the position of the lowest energetic ZPL can be different when Ce^{3+} is doped into LuAG. To understand the energy transfer between Tb^{3+} and Ce^{3+} in LuAG, it is important to determine the energy of the lowest 5d level of Ce^{3+}. If the lowest 5d level is higher in energy than the $^5D_4$ level, efficient trapping of the excitation energy by Ce^{3+} will be prevented.

In Figure 2 the excitation spectrum for the Ce^{3+} emission is shown, recorded at 293 K and at 4.5 K. The spectra exhibit two excitation bands with maxima at 445 and 340 nm which correspond to transitions to the two lowest energy levels of the five CF components in D_2 symmetry. The positions are similar to those for YAG:Ce. Both the width and relative intensities of these bands change with temperature. The 340 nm band is weaker at low temperatures, just as observed for YAG:Ce, due to the symmetry forbidden nature of the transition from the lowest CF component of the $^2F_{5/2}$ ground state to the second 5d state (around 340 nm). The transition from the second CF component of the $^2F_{5/2}$ ground state to the 5d state around 340 nm is symmetry allowed, which explains the increase in relative intensity of the 340 nm excitation band at higher temperatures when the second CF component is thermally populated. This observation is consistent with results for YAG:Ce.[9,12]

On the low energy side of both the 340 nm and the 450 nm excitation band, fine structure is observed at low temperature. The insets in Figure 2 present high resolution spectra of the band edges recorded at 4.5 K to show the fine structure in more detail. The spectra reveal ZPL of Ce^{3+} 5d bands as narrow

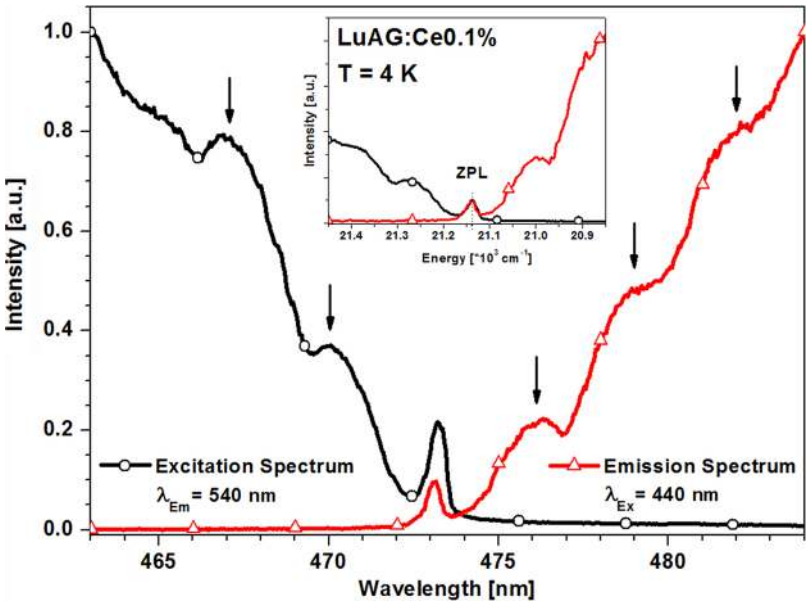

Figure 4. High resolution excitation and emission spectrum of LuAG:Ce0.1% showing ZPL overlap and vibronic replicas in the excitation and emission spectrum. Arrows mark the vibronic side bands.

peaks at 473.1 nm (21 138 cm^{-1}) and 354.2 nm (28 233 cm^{-1}) for the lowest and next higher Ce^{3+} 5d levels, respectively. Thus the CF splitting for the two lowest 5d CF levels of Ce^{3+} ion is 7100 cm^{-1}. This value is considerably smaller than the one observed for Ce^{3+} in YAG where ZPLs for the two lowest energetic 5d bands are situated at 489.2 and 347.2 nm, giving a splitting of 8360 cm^{-1}. The difference in splitting reflects the strong influence of the local coordination on the 5d CF splitting. It is, however, surprising that the larger CF splitting is observed for Ce^{3+} on the site with the larger ionic radius: the ionic radius of Y^{3+} in VIII coordination is 1.019 Å, whereas it is 0.977 Å for Lu^{3+}.[13] Usually, a larger CF splitting is observed for Ce^{3+} on a smaller site (smaller distances to the ligands give a larger CF splitting). For the garnet host a different trend is observed. Replacing the Y^{3+} ion (r_{VIII} = 1.019 Å) with the larger Gd^{3+} (r_{VIII} = 1.053 Å) has been shown before to result in larger CF splitting between the two lowest 5d levels and a red shift of the emission, both resulting from a higher CF splitting. In comparing YAG and LuAG, we observe the same trend: upon replacing Y^{3+} with the smaller Lu^{3+} ion, a blue shift of the emission is observed and the CF splitting decreases by 15%. Recent theoretical calculations on YAG:Ce,La have confirmed that replacing the smaller Y^{3+} ion by the larger La^{3+} ion (r_{VIII} = 1.160 Å) causes a blue shift and a larger CF splitting, in spite of local average expansion. First principles calculations reproduce the experimental observations and show how other effects (covalency, ligand field anisotropies) can explain the blue shift and decreasing CF splitting of the Ce^{3+} emission in LnAG when the ionic radius of the Ln^{3+} ion decreases.[14] The present quantitative results on the position and shift of ZPLs of the two lowest energy 5d bands for Ce^{3+} in LuAG may serve as an accurate input for comparison with future calculations.

The Ce^{3+} 5d−4f emission spectrum of LuAG:Ce0.1% is shown in Figure 3. The spectrum, recorded at 4.5 K, reveals two emission bands, split by ∼2000 cm^{-1}. This splitting is typically observed and related to the splitting of the ^2F ground state in a $^2F_{5/2}$ and a $^2F_{7/2}$ state. The high resolution spectrum in the inset reveals the presence of a ZPL at 473.10 nm, the same position observed in the low-temperature excitation spectrum. The relative intensity of the zero-phonon origin with respect to the higher energy emission band at 500 nm is small, approximately 1.2×10^{-4}.

In Figure 4 the onset of both the excitation and emission spectrum are plotted in one figure. The typical mirror symmetry in the ZPL at 473.1 nm is observed. For YAG:Ce similar behavior of spectra has been reported.[9] The vibronic progression observed in the low-temperature emission spectra for YAG:Ce revealed a strong coupling with 200 cm^{-1} vibrational modes. In the case of LuAG:Ce, the phonon energies observed in the emission spectra are lower, ∼130 cm^{-1} (see arrows in Figure 4). The lower energies of the vibrational modes can be explained by the higher mass of the Lu^{3+} ion relative to Y^{3+}.

The information gained from the high resolution excitation and emission spectra at low temperature enables the calculation of the Stokes' shift and the Huang−Rhys coupling parameter. Note that accurate calculations are possible only for spectra recorded for low dopant concentrations. Reabsorption, inhomogeneous broadening, and saturation effects prevent the observation of the ZPL and vibronic structure for higher concentrations and a red shift in the emission occurs as result of energy transfer and reabsorption of the high energy part of the emission. This results in an overestimation of the value for the Stokes' shift, as is often found in the literature. Also, to determine the 5d−$^2F_{5/2}$ emission maximum correctly, measurements should be performed at low temperature. At higher temperatures (e.g., 300 K) the spectral features related to emission from 5d state to $^2F_{5/2}$ and $^2F_{7/2}$ multiplets overlap and one broad band is observed, as shown in Figure 3, that prevents the determination of the Stokes' shift for the 5d → $^2F_{5/2}$ emission. The Stokes' shifts and the Huang−Rhys electron-coupling parameter S have been determined using different methods. A simple approach to calculate the Stokes' shift involves the determination of the energy difference between excitation (449.5 nm) and emission (501.5 nm) band maxima. This yields a value of 2312 cm^{-1} for the Stokes' shift of the 5d−4f emission in LuAG:Ce. Another method relies on doubling of the energy distance between the ZPL and the maximum of the

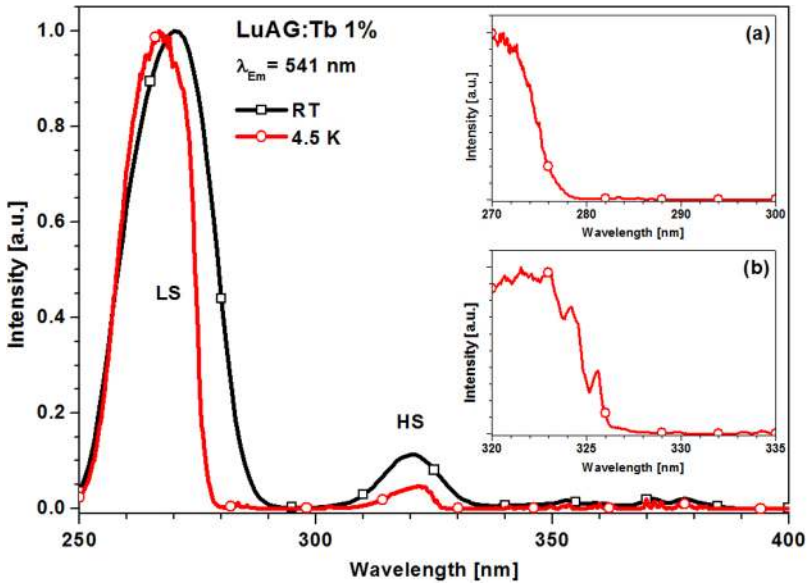

Figure 5. Excitation spectra of 541 nm emission in LuAG:Tb1% at 4.5 and 300 K. Insets a and b show high resolution spectra of the band onset, recorded at 4.5 K.

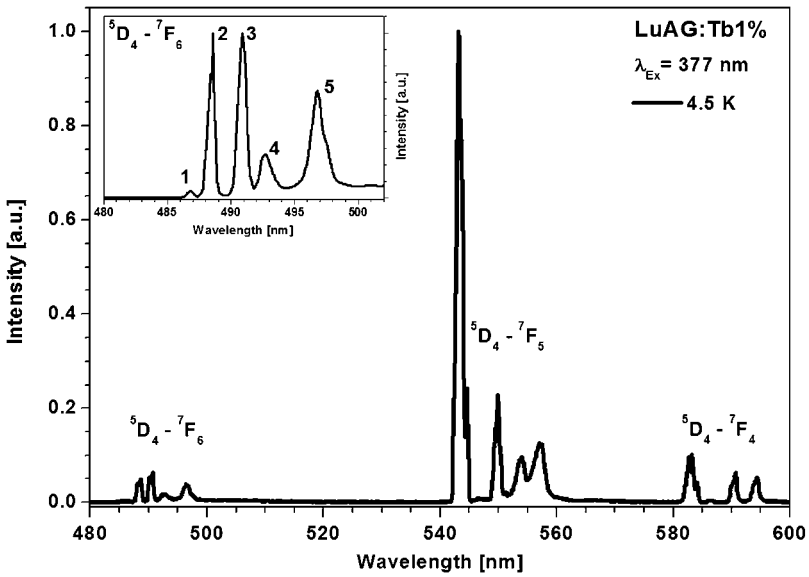

Figure 6. Emission spectrum LuAG:Tb1% recorded at 4.5 K for excitation at 377 nm. The inset shows the $^5D_4$–$^7F_6$ emission in more detail.

emission band. In this case a value of 2363 cm^{-1} is obtained. A third method involves the determination of the Huang–Rhys electron–phonon coupling parameter S from the relative intensity of the ZPL and using the equation for the Stokes' shift (SS): SS = $2S\cdot\hbar\omega$. The intensity of the ZPL (I_{ZPL}) and the total emission (I_0) intensity are related by $I_{ZPL} = I_0\cdot\exp(-S)$. The relative intensity of the ZPL is weak. After background subtraction, the intensity of the ZPL has been determined to be 1.2×10^{-4} from the total emission intensity of the 5d → $^2F_{5/2}$ emission band, which gives $S = 9$. This, together with the dominant phonon frequency of 130 cm^{-1}, gives the value of Stokes' shift of 2340 cm^{-1}. The values obtained for S and the Stokes' shift are consistent.

B. LuAG:Tb. The luminescence properties of the LuAG:Tb1% are studied to determine the energies of the 4f–5d absorption bands and the 4f–4f emission bands.

The excitation spectrum of Tb^{3+} doped LuAG for the $^5D_4$ emission at 541 nm is shown in Figure 5. The spectrum shows a strong excitation band at 270 nm and a weaker band at 320 nm. The stronger band is assigned to the spin-allowed 4f–5d transition to the low spin $4f^75d$ state (indicated by LS, low spin) and the weaker band is assigned to the transition to the spin-forbidden transition to the high spin (HS) $4f^75d$ state. At 4.5 K fine structure (ZPL and vibronic side bands) is observed for the HS band (see inset b in Figure 5) with the ZPL at 325.60 nm and vibrational energies of 130 cm^{-1}. Even though no ZPL is observed for the LS band, the HS–LS splitting can be calculated as 5388 cm^{-1} from the sharp onset of the LS band at 277 nm and the ZPL for the HS band at 325.6 nm. The value of HS–LS splitting obtained is smaller than what is typically observed for Tb^{3+} in other compounds. The average HS–LS splitting for Tb^{3+} reported by Dorenbos is 6300 cm^{-1}.[15] Meanwhile, in fluorides the HS–LS splitting close to 8000

cm^{-1} is typically observed. The large variation in HS−LS splitting has been related to the covalency of the host lattice.[16] In a more covalent host lattice the larger spatial extension of the 5d orbital will reduce the interaction with the 4f-core electrons resulting in a smaller HS−LS splitting. In this connection it is interesting to compare the results to those for YAG:Tb where the HS−LS splitting is calculated to be 5 285 cm^{-1} from the onset of the LS band at 280.7 nm and the ZPL for the HS band at 329.6 nm.[17] This indicates that the covalency for Ce^{3+} in the YAG lattice is larger than for Ce^{3+} in the LuAG lattice. The very low energy emission of Ce^{3+} in YAG can be explained by the lowering of the lowest energy emitting 5d state of Ce^{3+} by a combined effect of a large CF splitting and a high covalency. The Tb^{3+} 4f−5d absorption bands partly overlap with the intrinsic emission bands of LuAG typically observed as broad UV bands between 220 and 300 nm.[18,19] Efficient energy transfer from the host lattice to Tb^{3+} can be expected. Relaxation from the 5d states to the $^5D_4$ state will be fast. Whether or not efficient energy transfer from the $^5D_4$ state of Tb^{3+} to the 5d state of Ce^{3+} can occur, depends on the energy of the lowest $^5D_4$ state relative to the 5d state of Ce^{3+}.

To determine the position of the $^5D_4$ level, emission spectra of the 4f−4f emission were measured for LuAG:Tb in the visible part of the spectrum. In Figure 6 the emission spectrum of LuAG:Tb0.1% is shown under excitation at 377 nm in the $^5D_3$ level of Tb. The emission spectrum shows 4f−4f line emission corresponding to $^5D_4 \rightarrow {}^7F_{(6,5,4)}$ transitions. The structure of the $^5D_4$−$^7F_6$ emission presented in the high resolution inset comprises five emission lines that result from transitions from the lowest energy CF component of the $^5D_4$ level to different CF components of the $^7F_6$ ground level. The highest energy peak is at 486.85 nm, which is about 600 cm^{-1} lower in energy than the 5d state of Ce^{3+}.

C. LuAG:Ce,Tb. The information from the analysis of the luminescence spectra of the singly doped samples has been used to construct the energy diagram presented in the Figure 7. The part above 40 000 cm^{-1} is evaluated from the analysis of Figure 9 (vide infra). Relaxation after high-energy photon excitation (X- or γ-ray) consists of multiple excitation and relaxation processes. In the final stages, the energy dissipation in the doubly doped material will involve trapping of the elementary electronic excitations by both Ce^{3+} and Tb^{3+} ions. On the basis of the 600 cm^{-1} higher energy of the ZPL of the Ce^{3+} 5d state relative to the $^5D_4$ state of Tb^{3+}, energy transfer from Ce^{3+} to Tb^{3+} is expected rather than the desired $Tb^{3+} \rightarrow Ce^{3+}$ energy transfer. At low temperatures the Tb^{3+} emission is therefore expected to dominate. However, at higher temperatures the thermal equilibrium between the two states will allow for thermal population of the 5d state of Ce^{3+} (at room temperature the Boltzmann distribution predicts a 5% population of a state 600 cm^{-1} higher in energy) and because of the $\sim 10^4$−10^5 times higher decay rate of the 5d emission, the Ce^{3+} emission will dominate even though the 5d state is higher in energy than the $^5D_4$ state of Tb^{3+}. It is, however, important to realize that replacing a substantial fraction of Lu^{3+} (r_{VIII} = 0.977) by the larger Tb^{3+} (r_{VIII} = 1.04) will cause a red shift of the Ce^{3+} 5d level, based on the trend discussed above (larger CF for Ce^{3+} on a larger cation site) and the 5d state of Ce^{3+} may be shifted below the $^5D_4$ state of Tb^{3+} at high Tb^{3+} concentrations, making the energy transfer from Tb^{3+} to Ce^{3+} efficient even at low temperatures. A second contribution to efficient energy transfer at lower temperatures might be inhomogeneous broadening of the Ce^{3+} excitation bands.[20] At higher Tb concentrations the increased inhomogenous broadening can lead to lower energy Ce^{3+} sites due to specific arrangements of Lu^{3+} and Tb^{3+} around the Ce^{3+} ion which act as traps for the excitation energy at low temperatures.

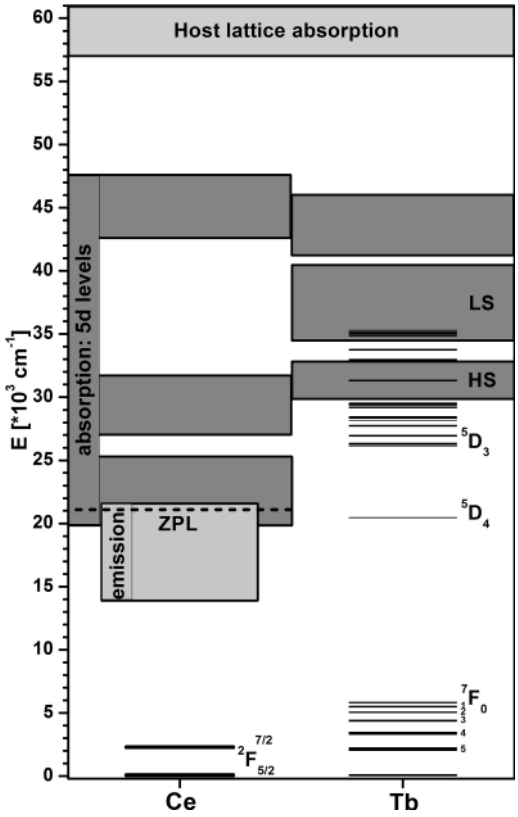

Figure 7. Diagram of the energy levels for Ce^{3+} and Tb^{3+} in LuAG.

To investigate the energy transfer between Ce^{3+} and Tb^{3+}, excitation and emission spectra were measured for LuAG:Ce,Tb samples where 25, 50, or 75% of the Lu^{3+} was replaced by Tb^{3+}. As an example, in Figure 8 emission spectra are shown for LuAG:Ce1%Tb50% at temperatures between 1.8 and 20 K. At 1.8 K the Tb^{3+} emission is clearly visible on top of the broad Ce^{3+} emission band. Upon raising the temperature, the Tb^{3+} emission decreases rapidly and above 5 K the Ce^{3+} emission dominates. Only a very weak Tb^{3+} emission line at 541 nm remains, superimposed on the Ce^{3+} 5d−4f emission band. Even at low temperatures no ZPL is observed on the high energy side of the Ce^{3+} 5d−4f emission band. This prevents a very accurate determination of the position of the lowest energy 5d state for Ce^{3+}. The fact that no ZPL is observed is due to inhomogeneous broadening caused by disorder in the Lu^{3+}−Tb^{3+} sublattice around the Ce^{3+} ions. The onset of the 5d−4f emission band at low temperatures is around 495 nm, which confirms the expected shift to lower energies due to the replacement of Lu^{3+} by the larger Tb^{3+} ion. In line with the 22 nm red shift of the ZPL the emission band maximum has also shifted to some 25 nm longer wavelengths. Due to the shift, the Ce^{3+} 5d level has energetically moved below the Tb^{3+} $^5D_4$ level, which remains around 487 nm because the position of the 4f levels is hardly influenced by the local surroundings. As a result of this, efficient trapping of the excitation energy by Ce^{3+} can be expected even at low temperature. This is in agreement with the observation of strong Ce^{3+} emission down to the lowest temperatures. Finally, it is interesting to understand the strong

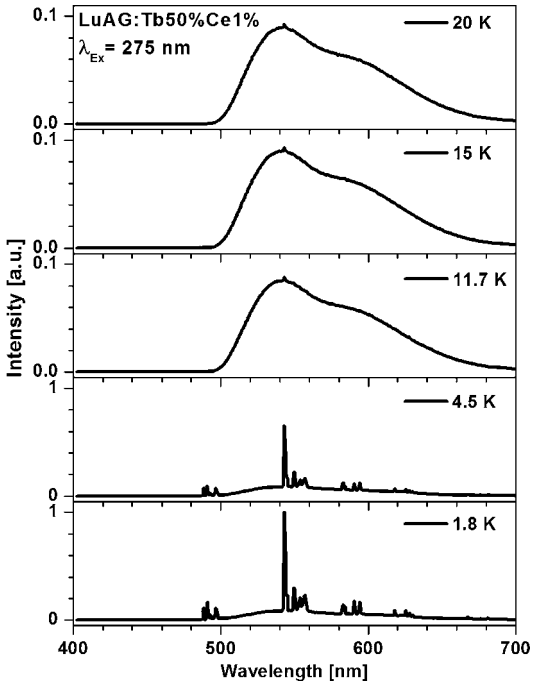

Figure 8. Temperature dependent emission spectra of LuAG:Ce1% Tb50% for excitation at 275 nm corresponding to the LS 5d band of Tb^{3+}. All spectra were normalized to the spectrum measured at 1.8 K.

decrease in the Tb^{3+} emission intensity between 1.8 and 10 K. At high Tb^{3+} concentrations, efficient energy migration over the Tb sublattice can be expected. Energy migration in concentrated rare earth systems has been extensively investigated in the past, especially for Eu^{3+}, Tb^{3+}, and Gd^{3+}.[21−24] For concentrations above the percolation point (where a 3D network of the optically active lanthanide ion is formed) energy transfer between lanthanide neighbors results in energy migration over the sublattice of the optically active ion to traps. In the present system, energy transfer between Tb^{3+} neighbors is efficient and the energy migrates over the $^5D_4$ levels of Tb^{3+} ions to traps, in this case Ce^{3+}. At the lowest temperatures (below 10 K) the energy migration is hampered due to small energy mismatches between neighboring Tb^{3+} ions resulting from inhomogeneous broadening. At higher temperatures phonon assistance (one- and two-phonon assisted energy transfer processes) helps to overcome the energy mismatch but at the lowest temperatures the phonons are frozen out and energy migration over the Tb^{3+} sublattice to Ce^{3+} becomes inefficient as the excitation energy is "trapped" by Tb^{3+} ions having the $^5D_4$ level at slightly lower energies. This can explain the observation of Tb^{3+} emission below 10 K and the strong temperature dependence between 1.8 and 10 K.[25,26] In the lowest temperature regime (T < 5K) it cannot be excluded that magnetic ordering further hampers energy migration, as for example observed in $TbAlO_3$ below the Neèl temperature of 3.8 K.[27,28]

The presence of efficient energy transfer from Tb^{3+} to Ce^{3+} is confirmed by the excitation spectra of the Ce^{3+} emission in (Lu,Tb)AG:Ce1% shown in Figure 9. The excitation spectra of codoped samples show, in addition to the 4f−5d absorption bands of Ce^{3+}, the 4f−5d excitation bands of Tb^{3+}, with strong spin-allowed absorption bands at 270 nm (also discussed above) and at 225 nm. The higher energy band at 225 nm is about 7500 cm^{-1} higher in energy than the 270 nm band, consistent with the CF splitting between the two lowest energy 5d states observed for Ce^{3+}. Upon increasing the Tb concentration from 25 to 50%, the 270 nm band shows a red shift whereas the 225 nm band shows a blue shift, in line with the observation of an increase in CF splitting observed when the smaller host lattice ion Lu^{3+} is replaced by the larger Tb^{3+} ions. Another observation that should be highlighted here is the dependence of host lattice intrinsic absorption edge on Tb^{3+} content. The pure Lu sample shows an onset of fundamental absorption around 185 nm that is in agreement with refs 18 and 19. Co-doping with Tb^{3+} leads to a gradual red shift of the onset and overlap with the 225 nm Tb^{3+} 4f−5d absorption band when the Tb^{3+} content reaches 75%.

In Figure 10 emission spectra at room temperature are shown for (Lu,Tb)AG:Ce1% with 0, 25, 50, or 75% Tb^{3+} for

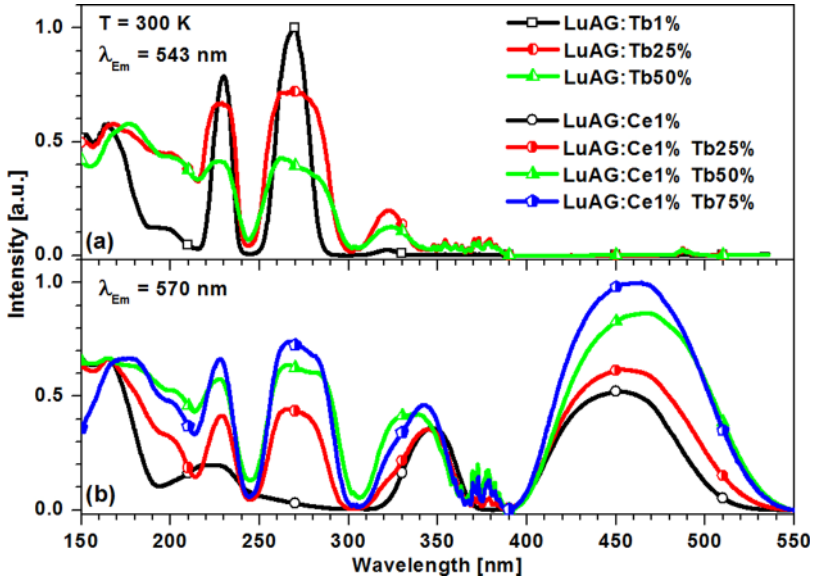

Figure 9. Room temperature excitation spectra of (a) the Tb^{3+} emission at 543 nm for LuAG with 1, 25, or 50% of Tb^{3+}, and (b) the Ce^{3+} emission at 540 nm for (Lu,Tb)AG:Ce1% where 0, 25, 50, or 75% of the Lu^{3+} ions have been replaced by Tb^{3+}.

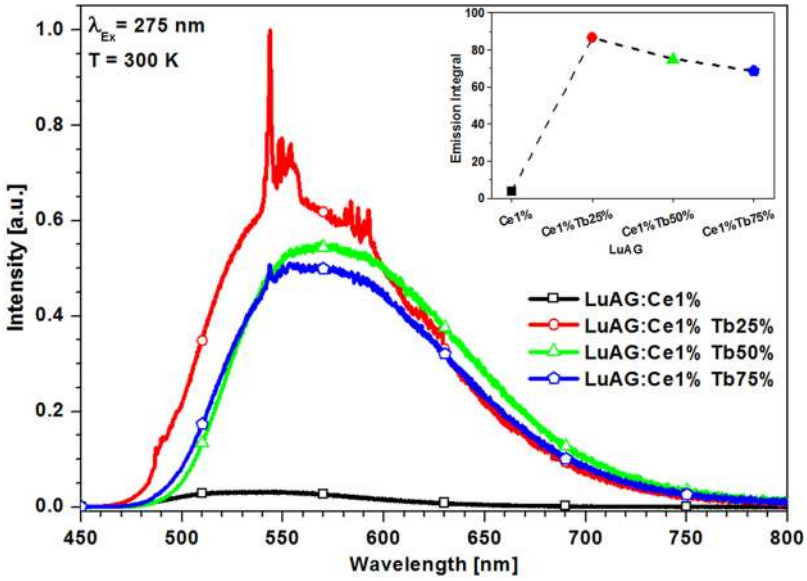

Figure 10. Room temperature emission spectra of Ce^{3+} and Tb^{3+} doped LuAG at excitation wavelength of 275 nm corresponding to LS 5d band of Tb^{3+}. The inset shows the integrated intensity in the 450 - 800 nm range.

excitation at 275 nm in the LS 5d band of Tb^{3+}. Analysis of these spectra together with decay time measurements shown in Figure 11, help to understand the energy transfer occurring between Tb^{3+} and Ce^{3+} ions in LuAG host lattice. Upon excitation at 275 nm in the sample doped with Ce^{3+} only, the emission intensity is weak, as Ce^{3+} is not efficiently excited at 270 nm (no 4f−5d absorption band). In all spectra the broad-band emission of Ce^{3+} dominates, showing that there is efficient energy transfer from Tb^{3+} to Ce^{3+}. In the case of LuAG:Ce1% Tb25%, Tb^{3+} 4f−4f line emissions on top of a broad Ce^{3+} emission band are visible. The relative intensity of the Tb^{3+} emission is approximately 3%. The Tb^{3+} emission peaks almost disappear when 50 or 75% Tb^{3+} is introduced. The small peak around 550 nm for the 75% Tb^{3+} sample is only ∼0.4% of the total emission intensity. The incomplete $Tb^{3+} \rightarrow Ce^{3+}$ energy transfer in the 25% samples indicates that energy migration over the diluted Tb sublattice is not efficient at 25% Tb^{3+} and a significant fraction of excited Tb^{3+} ions experiences an intracenter radiative relaxation. This is in agreement with previous work, where concentration quenching in (Y,Tb)AG was observed to set in at a Tb concentration of 40%.[29] At 50% and above, efficient energy migration over the Tb sublattice to Ce^{3+} ions occurs. Note that, after a continuous red shift for increasing Tb^{3+} concentration, the emission spectrum for the system with 75% Tb^{3+} shows a small blue shift in comparison with the system with 50% Tb^{3+}. This could be due to inhomogeneous broadening, which is expected to be largest for the composition with 50% Tb^{3+}.[20] The relative intensity of the Tb^{3+} emission can be estimated theoretically, assuming fast energy migration and an energy difference between the Ce^{3+} 5d level and the Tb^{3+} $^5D_4$ level that is much smaller than kT; i.e., the population of the Ce^{3+} and Tb^{3+} excited states is proportional to the concentrations of these ions. The relative emission intensities are then proportional to the concentration of ions and the radiative decay rates:

$$\frac{I_{Tb}}{I_{Ce}} = \frac{P_r^{Tb} \times C^{Tb}}{P_r^{Ce} \times C^{Ce}}$$

where I_{Tb} is the Tb^{3+} emission intensity, I_{Ce} is the Ce^{3+} emission intensity, P_r are the radiative decay rates (∼310 s^{-1} for the $^5D_4$ emission of Tb^{3+} and 16×10^6 s^{-1} for the 5d−4f emission of Ce^{3+} in LuAG) ,and C denotes the concentration. For the 75% Tb^{3+} samples, a relative intensity for the Tb^{3+}

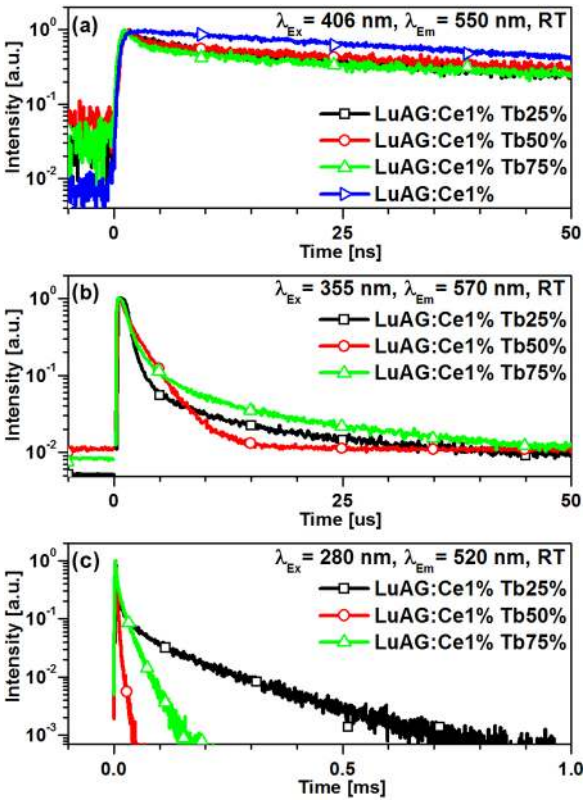

Figure 11. Room temperature luminescence decay of Ce^{3+} emission in LuAG:Ce,Tb in different time regimes: (a) ns time regime, λ_{exc} = 406 nm, λ_{em} = 550 nm; (b) μs time regime, λ_{exc} = 355 nm, λ_{em} = 570 nm and (c) ms time regime, λ_{exc} = 280 nm, λ_{em} = 520 nm. The compositions of the samples are indicated in the Figures.

dx.doi.org/10.1021/jp301337f | J. Phys. Chem. A 2012, 116, 8464−8474

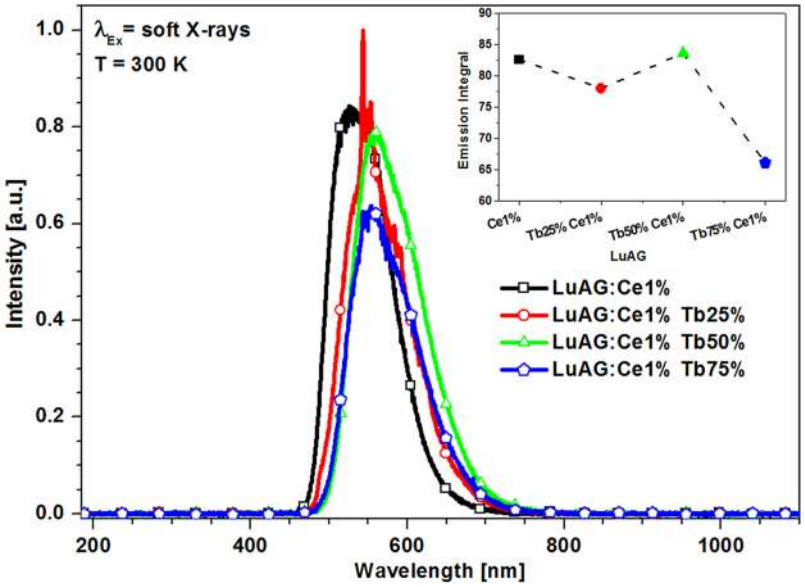

Figure 12. Emission spectra of LuAG:Ce,Tb monitored under soft X-ray excitation. The measurements were done at 300 K under identical experimental conditions.

emission is calculated to be 0.15% that is close to the experimentally obtained value of 0.4%.

To further analyze the energy transfer processes, luminescence decay curves can be recorded. Decay curves were measured at different time scales (nanosecond, microsecond, and millisecond) for the Ce^{3+} emission in samples codoped with different Tb^{3+} concentrations. In Figure 11a the decay curves are shown on a nanosecond time scale. For the samples without Tb^{3+} or with low Tb^{3+} concentration (1% or less) a single exponential decay is observed with τ = 63 ns. Upon increasing the Tb^{3+} concentration, an initial faster decay for the Ce^{3+} emission is observed due to energy transfer to Tb^{3+}. The fast component is more pronounced for the higher Tb concentrations. For the intermediate (microsecond) time scale (Figure 11b) the situation is complex. The initial decay is faster for the samples codoped with 25 and 75% Tb^{3+} and slower for the 50% Tb^{3+} sample. In the 10−40 μs regime, the situation is reversed. In the long (millisecond) time regime (Figure 11c), the sample with 25% Tb^{3+} shows a fast initial decay followed by a slow tail, confirming that the energy migration is hampered by the low Tb concentration. One of the reasons for existence of the slow decay components reflecting delayed feeding of the Ce^{3+} ions is connected with migration of excitation energy over the Tb^{3+} sublattice. The faster diffusion (above the percolation point) in the samples with 50 and 75% Tb^{3+} results in a rapid decay, and no millisecond decay component is observed. Another reason for the appearance of a millisecond decay tail can be connected with thermally induced detrapping of electrons from shallow traps into the conduction band followed by the delayed recombination at Ce^{3+} ions.[30−34] The longer decay in the 100−200 μs regime for the Ce^{3+} emission decay in the 75% Tb^{3+} sample compared with the 50% Tb^{3+} sample is consistent with the observations in Figure 11b but seems to be unusual. Normally, for higher donor concentration the faster energy migration leads to shorter decay times. However, the phenomenon observed may be connected with variation of trap depth due to lowering the conduction band. Particularly, some traps may become shallower and others become delocalized within the conduction band. The higher Tb^{3+} concentration can also explain a slightly longer decay, because in the case of thermal equilibrium the population of the $^5D_4$ state of Tb^{3+} is higher, but it cannot explain the lengthening observed in Figure 11b,c. In spite of extensive studies of the decay curves, also as a function of temperature, it has not been possible to explain all the observed luminescence decay behavior. This illustrates the complexity of the system, where due to the proximity of the Ce^{3+} and Tb^{3+} levels, both ions can act as donor and acceptor, with a very different decay rate, and also energy migration over the Tb^{3+} sublattice occurs. In addition, the energy mismatch varies as a function of Tb concentration due to the strong red shift of the 5d state of Ce^{3+} upon raising the Tb concentration. Because of this complexity, any further analysis of the decay curves is cumbersome. The observations presented above are in good qualitative agreement with the results recently presented by Setlur et al.[35] who provided a more quantitative analysis of the luminescence decay curves and found evidence of a shift from energy transfer through dipole−dipole transfer to exchange mediated energy transfer at higher Tb^{3+} concentrations.

The results presented above demonstrate that energy transfer from Tb^{3+} to Ce^{3+} is very efficient in LuAG:Ce,Tb. Energy losses in LuAG:Ce scintillators due to competition in trapping of the host lattice exciations between Ce^{3+} and defects may be prevented by codoping with Tb^{3+}. At high Tb^{3+} concentrations, trapping of the host lattice excitation will occur mainly at Tb^{3+} ions and will be followed by energy transfer to Ce^{3+} ions. To verify if this concept can be used to increase the actual efficiency of the scintillator materials above the typical 12 500 photons/MeV, luminescence efficiency measurements under soft X-ray excitation were done for (Lu,Tb)AG:Ce1% with 0, 25, 50, or 75% Tb. The results are shown in Figure 12. Emission spectra were recorded under identical conditions for excitation with a soft X-ray source. The spectra were recorded over a wide spectral range 200−1100 nm. Only in the region between 450 and 750 nm is emission observed. The integrated intensity under the emission curves is proportional to the light yield for the different materials. In the inset the integrated intensity is plotted for the different systems. The intensity is

approximately constant for the systems with 0−50% Tb. A lower light yield is observed for the sample codoped with 75% Tb^{3+}. The fact that there is no increase in the light yield indicates that the efficiency losses cannot be reduced by codoping with Tb under these conditions, which is in contrast to findings of Berkstresser et al. in the case of very low Tb^{3+} concentrations.[36] There are different models that could explain the observation of a constant to lower light yield on increasing the Tb concentration. Possibly, the energy losses are related to electron traps like Ce^{4+} and especially Tb^{4+}, which would trap a considerable fraction of electrons in the conduction band, which recombine nonradiatively with holes. We do, however, not have evidence for the presence of Ce^{4+} or Tb^{4+} based on diffuse reflection spectra. Both Ce^{3+} and Tb^{3+} can only act as hole trap, and as a result, energy losses by defects trapping electrons will not be reduced and give rise to the same fractional loss. The codoping only results in a shift of the initial excitation from Ce^{3+} to Tb^{3+} but because excitation of Tb^{3+} is followed by an almost 100% energy transfer to Ce^{3+}, the light output from Ce^{3+} is not affected. In the past, a variety of other shallow electron traps related to antisite defects have been identified in LuAG:Ce and this may explain the low light output upon X-ray excitation in our experiments.[31] It would be interesting to codope LuAG:Ce with a codopant that is capable of trapping electrons and transferring its excitation energy to Ce^{3+}. Eu^{3+} and Tm^{3+} are interesting candidates, although energy back-transfer from Ce^{3+} to Eu^{3+} or Tm^{3+} may prevent the observation of an increased Ce^{3+} light output. In the case Ce^{3+} to Eu^{3+} also electron transfer from excited Ce^{3+} to Eu^{3+} may occur, leading to quenching through a metal-to-metal charge transfer state. It has been shown recently that partial substation of Al^{3+} by Ga^{3+} reduces the trapping of free carriers due to shallow traps in $RE_3Al_5O_{12}$ without reducing the defect concentration but by shifting the conduction band edge.[32] Partial substitution of Al^{3+} by Ga^{3+} may therefore improve the scintillation properties of our material. Finally, the low light yield may be more general and inherent to the relatively high concentration of a number of different defects in LuAG (and other garnets). Part of the excitation energy is lost at defect sites before the activators are reached. If this is the case, only improved synthesis techniques aimed at reducing the defect concentrations will raise the light yield. Efforts in this direction are ongoing. An important aspect is reducing the temperature at which the single crystals are grown. The very high growth temperatures (e.g., ∼2000 °C in a typical Czochralski growth) are responsible for the high defect concentration in garnets, e.g., antisite defects.[37] An option is to make transparent ceramics from (nano)crystalline powders at lower temperatures (1500−1700 °C), as has been successfully demonstrated for YAG.[38,39] This route might lead to more efficient LuAG:Ce scintillators and may also lead to a further enhancement of the light yield upon codoping with Tb^{3+}.

IV. CONCLUSIONS

The luminescence properties of LuAG doped with Ce^{3+} and Tb^{3+} have been investigated and new insights into the energy level structure, energy transfer, and scintillation efficiency have been obtained. For Ce^{3+} in LuAG, ZPLs are observed at 473.1 nm (21 138 cm^{-1}) and 354.2 nm (28 233 cm^{-1}) for the lowest and next higher Ce^{3+} 5d levels, respectively. Vibronic structure is observed in both the excitation and emission spectra. The Huang−Rhys parameter (S = 9), phonon energy (130 cm^{-1}), and Stokes' shift (2300 cm^{-1}) have been determined from the low-temperature spectra. The luminescence spectra of Tb^{3+} show the characteristic $^5D_4$ emission lines in the green spectral region. The Tb^{3+} excitation spectra are dominated by $4f^8 \rightarrow 4f^7$ 5d transition. The spin-forbidden transition to the high spin (HS) state has a ZPL at 325.6 nm and shows vibronic structure, the spin-allowed transition to the low spin (LS) state has a sharp onset at 277 nm, giving a HS−LS splitting of 5400 cm^{-1}, which is lower than usually observed. The smaller splitting is explained by a smaller 5d−4f exchange coupling parameter J, which is reduced by covalency effects.

Measurements on the codoped system LuAG:Ce,Tb demonstrate efficient energy transfer from Tb^{3+} to Ce^{3+}. Replacement of the smaller Lu^{3+} ion by the larger Tb^{3+} ion induces a larger crystal splitting that shifts the lowest 5d state of Ce^{3+} to lower energies, even below the $^5D_4$ state of Tb^{3+}. The red shift of the Ce emission and larger CF splitting upon substitution of a smaller rare earth ion by a larger one has been observed previously in garnet host lattices and is opposite to the usual observation (larger CF splitting on a smaller cation site). In the codoped systems with 25, 50, and 75% of Tb^{3+}, efficient energy transfer to Ce^{3+} occurs down to the lowest temperatures. Luminescence lifetime measurements show that for 25% Tb^{3+} there is still slow (millisecond) feeding of the Ce^{3+} emission, which is not observed for 50 and 75% of Tb^{3+} where fast diffusion over the Tb^{3+} sublattice is followed by efficient energy transfer and emission from Ce^{3+}. A quantitative analysis of the decay curves to extract energy transfer parameters is hampered by the complicated situation of the nearly resonant $^5D_4$ state of Tb^{3+} and the 5d state of Ce^{3+} and rapid energy transfer between Ce^{3+}−Tb^{3+}, Tb^{3+}−Ce^{3+}, and Tb^{3+}−Tb^{3+}.

The light output under soft X-ray excitation has been shown to not increase upon codoping with Tb^{3+}, remaining well below the theoretical maximum based on the Bartram−Lempicki model. An increase in light output due to efficient trapping of host electronic excitations by Tb^{3+} followed by energy transfer to Ce^{3+} does not occur. Possibly, fast trapping of electrons in defect sites, followed by nonradiative recombination with holes, is responsible for the lower efficiency and these losses are not reduced by codoping with Tb^{3+}. To increase the scintillation efficiency, improved crystal growth techniques, reducing the defect concentration, are required.

■ AUTHOR INFORMATION

Corresponding Author

*E-mail: cees.ronda@philips.com.

Notes

The authors declare no competing financial interest.

■ ACKNOWLEDGMENTS

We thank Jack Boerekamp, Anne-Marie van Dongen, Wilco Keur and Sandra Spoor (Philips Research, Eindhoven, The Netherlands) and Laura Beekman (Philips Healthcare, Best, The Netherlands) for their contributions.

■ REFERENCES

(1) Conti, M.; Eriksson, L.; Rothfuss, H.; Melcher, C. L. *IEEE Trans. Nucl. Sci.* **2009**, *56*, 926−933.

(2) Ronda, C. R.; Gondek, J. M.; Goirand, E.; Jüstel, T.; Bettinelli, M.; Meijerink, A. *Proc. Mater. Res. Soc. Symp.* **2009**, *1111*, 1111−D08−01.

(3) Cherepy, N. J.; Kuntz, J. D.; Tillotson, T. M.; Speaks, D. T.; Payne, S. A.; Chai, B. H. T.; Porter-Chapman, Y.; Derenzo, S. E. *Nucl. Instrum. Methods* **2007**, *579*, 38−41.
(4) Autrata, R.; Schauer, P.; Kvapil, J.; Kvapil, J. *J. Phys. E: Sci. Instrum.* **1978**, *11*, 707−708.
(5) Srivastava, A. M.; Ronda, C. R. *Luminescence: Theory and Applications*; Wiley-VCH: Weinheim, 2007.
(6) Mares, J. A.; Beitlerova, A.; Nikl, M.; Solovieva, N.; D'ambrosio, C.; Blazek, K.; Maly, P.; Nejezchleb, K.; de Notaristefani, F. *Radiat. Meas.* **2004**, *38*, 353−357.
(7) Weber, M. J. *Nucl. Instrum. Methods Phys. Res., Sect. A* **2004**, *527*, 9−14.
(8) Shiang, J. J.; Setlur, A. A.; Srivastava, A. M.; Comanzo, H. A. US6630077 B2, 2003.
(9) Bachmann, V.; Ronda, C.; Meijerink, A. *Chem. Mater.* **2009**, *21*, 2077−2084.
(10) Korzhik, M. V.; Trower, W. P. *Appl. Phys. Lett.* **1995**, *66*, 2327−2328.
(11) Katelnikovas, A.; Barkauskas, J.; Ivanauskas, F.; Beganskiene, A.; Kareiva, A. *J. Sol-Gel Sci. Technol.* **2007**, *41*, 193−201.
(12) Robbins, D. J. *J. Electrochem. Soc.* **1979**, *126*, 1550−1555.
(13) Shannon, R. D.; Prewitt, C. T. *Acta Crystallogr., Sect. B: Struct. Sci.* **1969**, *25*, 925−946.
(14) Munoz-Garcia, A. B.; Pascual, J. L.; Barandiaran, Z.; Seijo, L. *Phys. Rev. B* **2010**, *82*, 064114.
(15) Dorenbos, P. *J. Lumin.* **2000**, *91*, 155−176.
(16) Dorenbos, P. *J. Phys.: Condens. Matter* **2003**, *15*, 8417−8434.
(17) Zych, A.; Ogiegło, J. M.; Ronda, C. R.; de Mello Donegá, C.; Meijerink, A. To be published.
(18) Babin, V.; Blazek, K.; Krasnikov, A.; Nejezchleb, K.; Nikl, M.; Savikhina, T.; Zazubovich, S. *Phys. Status Solidi* **2005**, *2*, 97−100.
(19) Zorenko, Yu.; Voloshinovskii, A.; Savchyn, V.; Voznyak, T.; Nikl, M.; Nejezchleb, K.; Mikhailin, V.; Kolobanov, V.; Spassky, D. *Phys. Status Solidi B* **2007**, *244*, 2180−2189.
(20) Setlur, A. A.; Srivastava, A. M. *Opt. Mater.* **2007**, *29*, 1647−1652.
(21) Meijerink, A.; Blasse, G. *J. Lumin.* **1989**, *43*, 283−289.
(22) Batentschuk, M.; Osvet, A.; Schierning, G.; Klier, A.; Schneider, J.; Winnacker, A. *Radiat. Meas.* **2004**, *38*, 539−543.
(23) Kiliaan, H. S.; Meijerink, A.; Blasse, G. *J. Lumin.* **1986**, *35*, 155−161.
(24) Smit, W. M. A.; Blasse, G. *J. Solid State Chem.* **1986**, *63*, 308−315.
(25) Blasse, G. *Prog. Solid State Chem.* **1988**, *18*, 79−171.
(26) Holstein, T.; Lyo, R. K.; Orbach, R. *Laser Spectroscopy of Solids*; Springer: Berlin, 1981.
(27) Joubert, M. F.; Linares, C.; Jacquier, B.; Wanklyn, B *J. Lumin.* **1984**, *31−32*, 90−92.
(28) Hüfner, S.; Holmes, L; Varsanyi, F.; Uitert van, L. G. *Phys. Rev.* **1968**, *171*, 507−513.
(29) Ziel van der, J. P.; Kopf, L.; Uitert van, L. G. *Phys. Rev. B.* **1972**, *6*, 615−623.
(30) Nikl, M.; Pejchal, J.; Mihokova, E.; Mares, J. A.; Ogino, H.; Yoshikawa, A.; Fukuda, T.; Vedda, A.; D'Ambrosio, C. *Appl. Phys. Lett.* **2006**, *88*, 141916.
(31) Nikl, M.; Vedda, A.; Fasoli, M.; Fontana, I.; Laguta, V. V.; Mihokova, E.; Pejchal, J.; Rosa, J.; Nejezchleb, K. *Phys. Rev. B* **2007**, *76*, 195121.
(32) Fasoli, M.; Vedda, A.; Nikl, M.; Jiang, C.; Uberuaga, B. P.; Andersson, D. A.; McClellan, K. J.; Stanek C. R. *Phys. Rev. B* **2011**, *84*, 081102(R).
(33) Kamada, K.; Endo, T.; Tsutumi, K.; Yanagida, T.; Fujimoto, Y.; Fukabori, A.; Yoshikawa, A.; Pejchal, J.; Nikl, M. *Cryst. Growth Des.* **2011**, *11*, 4484−4490.
(34) Kamada, K.; Yanagida, T.; Pejchal, J.; Nikl, M.; Endo, T.; Tsutumi, K.; Fujimoto, Y.; Fukabori, A.; Yoshikawa, A. *J. Phys. D Appl. Phys.* **2011**, *44*, 505104.
(35) Setlur, A. A.; Shiang, J. J.; Vess, C. J. *J. Phys. Chem. C* **2011**, *115*, 3475−3480.
(36) Berkstresser, G. W.; Shmulovich, J.; Huo, T. C. D.; Matulis, G *J. Electrochem. Soc.* **1987**, *134*, 2624−2628.
(37) Zhuravleva, M.; Yang, K.; Spurrier-Koschan, M.; Szupryczynski, P.; Yoshikawa, A.; Melcher, C. L. *J. Cryst. Growth* **2010**, *312*, 1244−1248.
(38) Tachiwaki, T.; Yoshinaka, M.; Hirota, K.; Ikegami, T.; Yamaguchi, O. *Solid State Commun.* **2001**, *119*, 603−606.
(39) Wen, L.; Sun, X.; Xiu, Z.; Chen, S.; Tsai, C.-T. *J. Eur. Ceram. Soc.* **2004**, *24*, 2681−2688.